EBioMedicine 42 (2019) 481–493

Contents lists available at ScienceDirect

EBioMedicine

journal homepage: www.ebiomedicine.com

EBioMedicine
Published by THE LANCET

Research paper

Arid1a regulates insulin sensitivity and lipid metabolism

Yu-Lan Qu [a,1], Chuan-Huai Deng [a,1], Qing Luo [a], Xue-Ying Shang [a], Jiao-Xiang Wu [a,b], Yi Shi [a], Lan Wang [a], Ze-Guang Han [a,*]

[a] Key Laboratory of Systems Biomedicine (Ministry of Education), Shanghai Center for Systems Biomedicine, Shanghai Jiao Tong University, Shanghai 200240, China
[b] Collaborative Innovation Center of Systems Biomedicine of Rui-Jin Hospital, Shanghai Jiao Tong University School of Medicine, Shanghai, China

ARTICLE INFO

Article history:
Received 16 January 2019
Received in revised form 27 February 2019
Accepted 8 March 2019
Available online 14 March 2019

Keywords:
Arid1a
Steatosis
Insulin resistance
Fatty acid oxidation
PPARα

ABSTRACT

Background: Although significant progress has been made in understanding the mechanisms of steatosis and insulin resistance, the physiological functions of the epigenetic regulators in these processes remain largely elusive.
Methods: Hepatocyte-specific *Arid1a* knockout mice were administrated with high-fat diet (HFD) for 12 weeks, then insulin sensitivity was assessed by glucose tolerance test (GTT) and insulin tolerance test (ITT). The metabolism-related indicators were determined by employing a variety of biological methods, including histology, real-time PCR, enzyme-linked immunosorbent assay (ELISA), Western blotting assay, Chromatin immunoprecipitation (ChIP), RNA-seq and assay for Transposase-Accessible Chromatin with high-throughput sequencing (ATAC-seq).
Findings: Hepatocyte-specific *Arid1a* deletion significantly increases susceptibility to develop hepatic steatosis, insulin resistance and inflammation in mice fed a HFD. In vitro, *Arid1a* deletion in isolated hepatocytes directly leads to free fatty acid-induced lipid accumulation and insulin resistance. Mechanically, *Arid1a* deficiency impairs fatty acid oxidation by downregulating PPARα and altering the epigenetic landscape of some metabolism genes.
Interpretation: These findings reveal that targeting Arid1a might be a promising therapeutic strategy for liver steatosis and insulin resistance.
Fund: This work was supported by National Natural Science Foundation of China (81672772 and 81472621), China National Science and Technology Major Project for Prevention and Treatment of Infectious Diseases (No.2017ZX 10203207) and National Program on Key Research Project of China (grant no. 2016YFC0902701).

1. Introduction

Obesity has become a major epidemic around the world, contributing to an increased risk for metabolic syndrome, nonalcoholic fatty liver disease (NAFLD), type 2 diabetes (T2D), cancer and heart disease. Insulin resistance is closely associated with the pathogenesis of these modern diseases. Thus, understanding the pathogenesis of this process has become increasingly important to find new therapeutic targets. The association between lipid accumulation and insulin resistance is widely accepted, and ectopic lipid accumulation can lead to hepatic steatosis and insulin resistance [2]. Fatty acid oxidation (FAO) is a multistep process that involves the degradation of fatty acids (FAs) by sequential removal of two-carbon units from the acyl chain to produce acetyl-CoA. There are compelling evidences showing that undermined hepatic FAO is one of the central processes in hepatic lipid disorders [3]. Inadequate oxidation of fatty acid can lead to aberrant lipid accumulation and massive steatosis [4]. However, the underlying mechanisms for this process are complex, multifactorial and heterogeneous, which hinder the exploration of exact pathological processes and therapeutic methods.

SWI/SNF chromatin remodeling complex manipulates the accessibility of regulatory transcriptional factors and thereby controls the transcriptional activation and repression of some genes related to physiological functions [5,6]. So far, most previous studies of SWI/SNF complex are focused on cell proliferation, stem cell differentiation, genomic stability, DNA damage and repair, and the effects of SWI/SNF complex members on nutrient metabolism remain unclear. It was reported that hepatocyte-specific deletion of SNF5, another subunit of SWI/SNF complex, caused glycogen storage deficiency and energetic

Abbreviations: FAO, fatty acid oxidation; FFAs, free fatty acids; HFD, high fat diet; CD, chow diet; GTT, glucose tolerance test; ITT, insulin tolerance test; LKO, liver-specific knockout; HE, hematoxylin and eosin; TG, triglyceride; TCHO, total cholesterol; NEFA, non-esterified fatty acid; ALT, alanine amino transferase; AST, aspartate amino transferase; ALP, alkaline phosphatase; KEGG, Kyoto Encyclopedia of Genes and Genomes; GO, gene ontology; OA, oleic acid; PA, palmitic acid.

* Corresponding author at: Key Laboratory of Systems Biomedicine (Ministry of Education), Shanghai Center for Systems Biomedicine, Shanghai Jiao Tong University, 800 Dongchuan Road, Shanghai 200240, China.
E-mail address: hanzg@sjtu.edu.cn (Z.-G. Han).
[1] These authors contributed equally to this work.

https://doi.org/10.1016/j.ebiom.2019.03.021

Research in context

Evidence before this study

Our group previously demonstrated that hepatocyte-specific *Arid1a* deficiency initiated mouse steatohepatitis and HCC [1], suggesting that *Arid1a* might participate in lipid metabolism. In addition, other members in SWI/SNF complex, including SNF5, BAF60a and BAF60c were also involved in metabolism regulation, implying that Arid1a might play a role in HFD-induced steatosis and insulin resistance.

Added value of this study

Abnormal lipid metabolism in the liver leads to hepatic steatosis, which further promotes insulin resistance and inflammation, leading to several metabolic-related diseases. We demonstrated that hepatic-specific *Arid1a* deletion aggravated HFD-induced steatosis and insulin resistance. Mechanically, *Arid1a* loss disrupted the epigenetic landscape of key metabolic genes and Pparα-mediated fatty acid oxidation (FAO) process, offering new insight that Arid1a could be a promising target for treatment of hepatic steatosis, fibrosis and insulin resistance.

Implications of all the available evidence

Our data have disclosed a novel epigenetic regulator that contributed to insulin resistance and steatosis, implying that targeting Arid1a might be a promising therapeutic strategy for metabolic related disorders.

metabolism impairment [7]. Baf60a and Baf60c regulated metabolic gene programs in the liver and skeletal muscle [8,9]. In addition, Baf60a controlled the transcriptional programs of some genes responsible for hepatic bile acid synthesis and intestinal cholesterol absorption [10]. Moreover, expression of BAF60a could stimulate fatty acid β-oxidation in cultured hepatocytes and ameliorated hepatic steatosis in vivo [11].

ARID1A, also known as BAF250A, a subunit of SWI/SNF chromatin remodeling complex, may facilitate the access of transcription factors and regulatory proteins to genomic DNA. Loss of ARID1A may result in the structural and functional alterations of SWI/SNF complex, which leads to transcriptional dysfunction through disruption of nucleosome sliding activity, assembly of variant SWI/SNF complexes, targeting to specific genomic loci, and recruitment of coactivator/corepressor activities [12–17]. Our group previously demonstrated that hepatocyte-specific *Arid1a* deficiency initiated mouse steatohepatitis and HCC [1], suggesting that *Arid1a* might participate in lipid metabolism, however, the exact pathological process and the underlying molecular mechanism were unclear. Recently, Moore et al. showed liver-specific *Arid1a* deletion caused the development of age-dependent fatty liver disease, and combined *Arid1a* and *Pten* deletion showed accelerated fatty liver disease progression [18]. In this study, we employed hepatocyte-specific *Arid1a* knockout mice administrated with high-fat diet (HFD), and proved that wild type *Arid1a* protected mice against hepatic steatosis and insulin resistance. Mechanistically, *Arid1a* directly controlled the transcriptional activation of multiple metabolic genes by erasing H3K4me3 marks, and downregulated *PPARα* which thus inhibited fatty acid oxidation to regulate lipid metabolism and insulin sensitivity. In general, our findings that *Arid1a* may regulate lipid metabolism via directly or indirectly modulating the transcription of fatty acid oxidation-related genes provide a promising therapeutic approach for lipid accumulation and insulin resistance.

2. Materials and methods

2.1. Mice and diets

Arid1a^{LKO} mice were generated by mating *Arid1a*$^{Flox/Flox}$ mice (kindly provided by Zhong Wang at the Cardiovascular Research Center, Massachusetts General Hospital, Harvard Medical School) with Albumin-Cre mice (from the Jackson Laboratory). *Arid1a*$^{Flox/Flox}$ animals were used as controls. Six week-old *Arid1a*^{LKO} and *Arid1a*$^{Flox/Flox}$ mice were given free access to a HFD (composed of 59% fat, 15% protein, and 26% carbohydrates based on caloric content) or chow diet (CD) (protein, 20%; fat, 10%; carbohydrates, 70%) for 12 weeks. All animal experiments were approved by the Animal Care and Use Committee of Shanghai Jiao Tong University, and all the procedures were conducted in compliance with institutional guidelines and protocols.

2.2. Blood parameters

The concentrations of the hepatic enzymes alanine amino transferase (ALT), aspartate amino transferase (AST) and alkaline phosphatase (ALP) were analyzed using a spectrophotometer (Chemix 180i) according to manufacturer's instructions. Insulin plasma levels were determined using mouse insulin ELISA kit (Millipore). The levels of the serum inflammatory indicators were measured by ELISA kits (BD Bioscience).

2.3. Lipid parameters

Commercial kits were used to measure the liver triglyceride (TG), total cholesterol (TC) and nonesterified fatty acid (NEFA) contents in the liver according to the manufacturer's instructions (290-63701 for TG, 294-65801 for TC, 294-63601 for NEFA, Wako). Serum lipids were analyzed using a spectrophotometer (Chemix 180i) according to manufacturer's instructions.

2.4. Glucose and insulin tolerance tests

Glucose tolerance tests (GTT) were performed in mice that were fed with either CD or HFD for 12 weeks. One week later, the same mice were used for insulin tolerance tests (ITT). For GTT, mice were fasted for 16 h. After measuring the baseline blood glucose level via a tail nick using a glucometer, 1.5 g/kg glucose was administered via intraperitoneal injection, and glucose levels were measured 0,15,30,45,60,90 and 120 min after glucose injection. For ITT, 6 h fasted mice were injected intraperitoneally with recombinant human insulin at 1 U/kg and their blood glucose concentrations were determined 0,15,30,45,60,90 and 120 min after insulin injection.

2.5. Quantitative real-time PCR analysis

RNA extracted from liver or hepatocytes were subjected to reverse transcription and subsequent PCR using a real-time PCR system (ABI). PCR primer sequences are listed in Supplemental Table 1. Expression of the respective genes was normalized to β-Actin as an internal control.

2.6. Primary hepatocyte isolation, cultivation and treatment

Primary hepatocytes were isolated from 6- to 8-week-old mice following the steps reported previously [19]. Hepatocytes were cultured in Dulbecco's modified Eagle's medium contained 10% fetal bovine serum (FBS) and 1% penicillin-streptomycin in a humidified incubator supplied with 5% CO_2 at 37 °C. To stimulate insulin signaling, hepatocytes were stimulated with insulin 10 nM for indicated time. For lipid accumulation in vitro, hepatocytes were treated with 0.2 mM palmitate acid or 0.08 mM oleic acid for 24 h.

2.7. Plasmid construction and transfection

The plasmids encoding T7-ARID1A was purchased from Addgene and reconstructed by our lab. The plasmid expressing flag-tagged human PPARα was constructed by cloning the mouse PPARα cDNA into the pcDNA3.0 vector. The plasmid expressing HA-tagged human MTTP was constructed by cloning the MTTP cDNA into the pcDNA3.0 vector. Transfection assays for plasmids were performed using Lipofectamine 2000 (Invitrogen) according to the manufacturer's protocol.

2.8. Histological analysis

Sirius red (Sigma-Aldrich) staining was performed using paraffin-prepared liver sections to determine the fibrosis of the tissues. Liver sections were embedded in paraffin and stained with hematoxylin and eosin (H&E) to visualize adipocytes and inflammatory cells in the tissues. Frozen liver sections of 10 μm were fixed in formalin and then rinsed with 60% isopropanol. After staining with freshly prepared Oil-red O solution (Sigma-Aldrich) for 10 min, the sections were rinsed again with 60% isopropanol. Sections or cells were analyzed by inverted microscope (Olympus).

2.9. Western blotting

After extracted from liver samples or cultured cells, each protein sample (50 mg) was subjected to SDS/PAGE and transferred to nitrocellulose membrane. Then the corresponding primary and secondary antibodies were incubated to visualize the protein. Antibodies used in western blot analysis included anti-ARID1A (CST, Cat # 12354, RRID: AB_2637010), anti-phospho-AKTS473 (CST, Cat # 9271, RRID: AB_329825), anti-phospho-GSK3β (CST, Cat # 9323, RRID: AB_2115201), anti-AKT (CST, Cat # 9272, RRID: AB_329827) anti-GSK3β (CST, Cat # 9315, RRID: AB_490890), anti-PPARα (Abcam, Cat # ab2779, RRID: AB_303292), anti-Flag (Sigma-Aldrich, Cat # F1804, RRID: AB_262044), anti-T7 (Abcam, Cat # ab9138, RRID: AB_307038), anti-β-actin (Sigma-Aldrich, Cat # A4700, RRID: AB_476730).

2.10. ChIP

Chromatin immunoprecipitation (ChIP) assay was performed according to the protocol developed by Upstate Biotechnology. Briefly, chromatin lysates were prepared from hepatocytes after crosslinking with 1% formaldehyde. The samples were precleared with Protein-G agarose beads and immunoprecipitated using antibodies against Arid1a (Santa Cruz, Cat # sc32761-x, RRID: AB_673396), H3K4me3 (Abcam, Cat # 8580, RRID: AB_306649), BRG1 (Santa Cruz, Cat # sc17796, RRID: AB_626762) or control IgG in the presence of BSA and salmon sperm DNA. Beads were extensively washed before reverse crosslinking. DNA was purified using a PCR Purification Kit and subsequently analyzed by qPCR using primers located on the *Acox1* and *Cpt1a* promoter.

2.11. RNA-Seq

Total RNA-seq was performed on three independent biological replicates per condition. Samples from different conditions were processed together to prevent batch effects. For each sample, 10 million cells were used to extract total RNA and produce RNA-seq libraries. Raw sequencing reads were trimmed by Trimmomatic (v0.36) to remove adapters and low quality sequences. The filtered reads were aligned to the GRCm38 UCSC annotated transcripts via Tophat (v2.1.0) [20]. Transcripts were then assembled, counted and normalized with the Cufflinks suit (v2.2.1) [21]. Differentiated expressed genes were analyzed by Cuffdiff in the Cufflinks suit, using p value <.05 and fold change >1.5 as cutoff. Heatmaps were generated by using R package pheatmap (1.0.10).

Gene ontology and KEGG pathway enrichment analyses were performed using DAVID (v6.8) with the differentially expressed gene lists. Gene set enrichment analysis (GSEA v3.0) was performed using the normalized expression values [22]. The raw sequencing data of RNA-seq has been deposited to NCBI SRA database with the accession number PRJNA514189.

2.12. ATAC-seq

Cells were harvested and subjected for ATAC-seq analysis as previously described [23]. Briefly, 50, 000 cells were washed with cold PBS and cell membrane was lysed in lysis buffer (10 mM Tris-HCl, pH 7.4, 10 mM NaCl, 3 mM $MgCl_2$, 0.1% Nonidet P-40). After centrifugation, cell pellets were resuspended and incubated in transposition mix containing Tn5 transposase (Illumina) at 37 °C for 30 min. Purified DNA was then ligated with adapters and amplified 11 total cycles. Libraries were purified with AMPure beads (Beckman Coulter) to remove contaminating primer dimers. Libraries were then sequenced on Illumina X-Ten system with 150 bp paired-end sequencing strategy.

For ATAC-seq data analysis, Illumina adapters and low-quality reads were trimmed by Trimmomatic (v0.36) (Trimmomatic: a flexible trimmer for illumina sequence data). Afterwards, all reads for each sample were combined and aligned to mouse reference build GRCm38 using bwa (v0.7.11) with default settings. 40 to 65 million reads were obtained from the libraries of the primary mouse liver cells. Low quality reads (mapping quality <20) and reads mapping to mitochondrial DNA were removed using samtools (v1.6). Duplicates were excluded using Picard Tools (v1.4.5). Between 11 and 25 million high-quality reads per sample that mapped to genomic DNA were obtained for mouse primary liver cells. All mapped reads were offset by +4 bp for the +strand and -5 bp for the –strand (Transposition of native chromatin for fast and sensitive epigenomic profiling of open chromatin, DNA-binding proteins and nucleosome position) using bedtools (v2.25.0). Libraries of the same condition were merged for subsequent analyses. Peaks were called for each sample using MACS2 (Model-based analysis of ChIP-Seq (MACS) (v2.1.1.20160309) using parameter "-nomodel-shift 100-extsize 200". The peaks with $p < .01$ for each group in the same cell line were merged for searching differential peaks. Differential peak calling, as well as peak annotation and motif analysis were performed using HOMER (v4.9.1) with default settings. Fold change larger than 2 was set as the cutoff for differential peak identification. Sequencing signals were generated by transforming the mapping files into bigwig tracks, which was visualized in the Integrated Genomic Viewer (IGV). Signal heat maps centered around peaks were generated using deep Tools (v 2.5.3). The raw sequencing data of ATAC-seq has been deposited to NCBI SRA database with the accession number PRJNA514189.

2.13. Statistics

All statistical analyses were performed using Graphpad prism software (version 19.0), and all data are expressed as the mean ± standard deviation. For data with a normal distribution and homogeneity of variance, two-tailed student t-tests were used to evaluate significant differences between two groups, P values <.05 were considered significant. * $P < .05$; ** $P < .01$; *** $P < .001$.

3. Results

3.1. Arid1a is required for regulating insulin sensitivity and glucose tolerance

To directly address the effect of *Arid1a* deletion on glucose homeostasis and insulin sensitivity, liver-specific *Arid1a* knockout ($Arid1a^{LKO}$) mice and $Arid1a^{F/F}$ mice were placed on a normal chow diet (CD) or high-fat diet (HFD), and then metabolic phenotypes of these mice

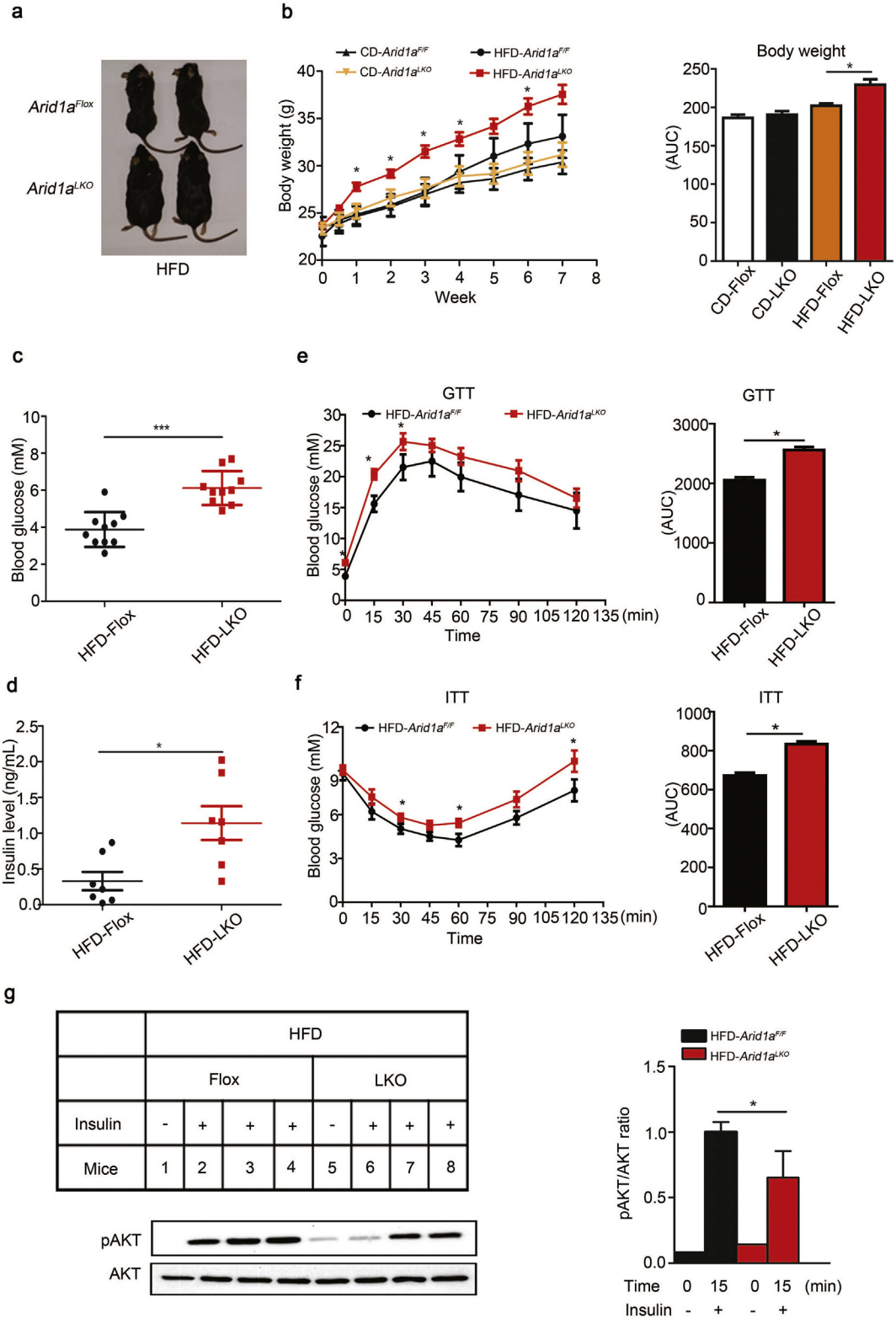

Fig. 1. Hepatic *Arid1a* deletion alters glucose tolerance and promotes insulin resistance. (a) Representative images of *Arid1a*^{LKO} and *Arid1a*$^{F/F}$ littermates after HFD feeding for 12 weeks. (b) Left, growth curve of *Arid1a*^{LKO} and *Arid1a*$^{F/F}$ littermates fed a CD or HFD; Right, quantitation of body weight (n = 9–10). (c) Fasting blood glucose level of mice fed a HFD (n = 10). (d) ELISA-determined fasting serum insulin level of mice fed a HFD (n = 7). (e) Left, measurement of plasma glucose during glucose tolerance test (GTT) of mice fed a HFD; Right, the calculated AUCs (area under curves) in *Arid1a*^{LKO} and *Arid1a*$^{F/F}$ mice fed a HFD (n = 8–10). (f) Left, measurement of plasma glucose during insulin tolerance test (ITT) of mice fed a HFD; Right, the calculated AUCs (area under curves) in *Arid1a*^{LKO} and *Arid1a*$^{F/F}$ mice fed a HFD (n = 8–10). (g) Left, total and phosphorylated Akt levels in the livers of *Arid1a*^{LKO} and *Arid1a*$^{F/F}$ mice fed a HFD after intraperitoneal insulin injection; Right, the expression levels of the protein as phosphorylated- to total-protein ratio (n = 3). Statistical analysis was performed. Values are mean ± SD. (* $P < .05$; *** $P < .001$).

were characterized. Interestingly, despite of similar food intake (Supplementary Fig. 1a), *Arid1a*^{LKO} mice gained much more body weights than *Arid1a*$^{F/F}$ mice when placed on a HFD. However, no difference was statistically identified between the *Arid1a*^{LKO} and *Arid1a*$^{F/F}$ littermates fed a CD (Fig. 1a–b). In parallel, compared to *Arid1a*$^{F/F}$ littermates fed a HFD, *Arid1a*^{LKO} mice showed significantly elevated levels of fasting blood glucose (Fig. 1c) and insulin (Fig. 1d), as well as the markedly decreased glucose tolerance via glucose tolerance test (GTT) (Fig. 1e) and insulin sensitivity shown by insulin tolerance test (ITT) (Fig. 1f). Furthermore, insulin sensitivity was assessed by measuring the phosphorylated Protein Kinase B (pAkt) level in livers of *Arid1a*^{LKO} mice fed a HFD. As expected, after injection of insulin, pAkt level was significantly decreased in the livers of *Arid1a*^{LKO} mice (Fig. 1g). However, no significant difference in blood glucose and insulin levels were found between *Arid1a*^{LKO} and *Arid1a*$^{F/F}$ group fed a CD during GTT and ITT tests (Supplementary Fig. 1b–e). Collectively, these data indicate that hepatocyte-specific *Arid1a* deletion damages insulin sensitivity, thereby leading to insulin resistance and impaired glucose tolerance of *Arid1a*^{LKO} mice under HFD challenge.

3.2. HFD aggravates Arid1a deficiency-induced hepatic steatosis, fibrosis and inflammation

Hepatic steatosis is strongly associated with hepatic insulin resistance. We next carried out histological comparisons between the livers from 4-month old *Arid1a*^{LKO} and *Arid1a*$^{F/F}$ mice. As compared to *Arid1a*$^{F/F}$ mice, *Arid1a*^{LKO} mice fed a CD exhibited hepatic dysplasia, steatosis and fibrosis [1]. HFD stimulation significantly aggravated these phenotypes of *Arid1a*^{LKO} mice, as evidenced by quantitatively analyses on histology according to the degree of steatosis, lobular inflammation, and hepatocyte ballooning (Fig. 2a and b). In addition, more lipid droplets were accumulated in the livers of *Arid1a*^{LKO} mice challenged with HFD, as visualized by Oil Red O staining (Fig. 2c). In parallel with these morphologic changes, the *Arid1a*^{LKO} mice fed a HFD exhibited worse liver function, as indicated by significant elevation of serum AST, ALT and ALP levels (Fig. 2d-f). Moreover, the mRNA levels of inflammatory-related genes including *Tnfα, Arg1, Mcp1 and Cd11b* were also markedly elevated in HFD-fed *Arid1a*^{LKO} mice compared to those of the *Arid1a*$^{F/F}$ mice (Fig. 2g). Correspondingly, blood concentration of TNF-α (Fig. 2h) was also significantly increased in obese *Arid1a*^{LKO} mice, although serum level of IL-6 had no significant change (Fig. 2i). Taken together, these data indicate that HFD aggravates *Arid1a* deficiency-induced hepatic steatosis, fibrosis and inflammation, suggesting that the *Arid1a* deficiency induces dysregulation of lipid mechanism.

Non-alcoholic steatohepatitis (NASH) is characterized by hepatic steatosis, insulin resistance and inflammation. To test the relationship between *Arid1a* expression and steatosis, fibrosis, as well as insulin resistance phenotypes in humans, we further analyzed a publically available transcriptomic data set of healthy people and NASH patients (GSE37031). As compared with healthy people, *Arid1a* is downregulated in NASH patients (Supplementary information, Fig. 2), suggesting that alterations in *Arid1a* expression may impact NASH development in humans.

3.3. Arid1a deletion leads to hepatic steatosis possibly through FAO impairment

Metabolic imbalance between lipid acquisition and removal in the liver is the first step in the pathophysiology of steatosis [24]. To explore the effects of *Arid1a* on hepatic lipid metabolism, the mice were fed with a CD or HFD for 12 weeks and then sacrificed to observe their phenotypes. Significantly, the liver weights of the *Arid1a*^{LKO} mice fed a HFD were much higher than those of the *Arid1a*$^{F/F}$ mice (Fig. 3a). Additionally, both subcutaneous white adipose tissue (WAT) and inguinal WAT fat pads were larger in *Arid1a*^{LKO} mice (Fig. 3b and c), indicative of decreased adipose tissue homeostasis. Afterwards, blood lipid testing revealed that plasma cholesterol (TCHO), low-density lipoprotein cholesterol (LDL), as well as high-density lipoprotein cholesterol (HDL) levels, but not non-esterified fatty acids (NEFA) were much higher in *Arid1a*^{LKO} animals (Fig. 3d–f). Surprisingly, plasma triglycerides (TG) of *Arid1a*^{LKO} mice was reduced (Fig. 3d). Furthermore, we determined liver lipids. TCHO and TG contents in the livers from HFD-fed *Arid1a*^{LKO} mice were significantly increased, and hepatic TG in *Arid1a*^{LKO} mice was even 8-fold higher than those in *Arid1a*$^{F/F}$ mice (Fig. 3g), indicating that the hyperlipidemia of *Arid1a*^{LKO} mice on HFD is likely caused by hepatic *Arid1a* loss.

Based on the observation that dysregulated lipid metabolism was induced by *Arid1a* deletion, we assessed transcriptional expression of genes related to lipid acquisition and removal, including fatty acid synthesis, oxidation and TG secretion. Whereas quantitative reverse transcriptase PCR (qRT-PCR) analysis in livers of mice fed a CD showed a trend of decreased gene expression related to fatty acid oxidation and secretion in *Arid1a*^{LKO} mice (Supplementary Fig. 3a-c), the mRNAs encoded by these genes involved in FAO (*Pparα*, *Cpt1a*, *Acox1*, *Pgc1α*, *Hmgcs2*, etc.) and secretion (*Mttp*) were significantly reduced in the *Arid1a*^{LKO} mice with HFD administration. However, there was no obvious difference of gene expression related to fatty acid synthesis (*Fas*, *Acc1*, *Pparγ*, *Sreb1c* and *Chrebp*) between *Arid1a*^{LKO} and *Arid1a*$^{F/F}$ mice (Fig. 3h–j), suggesting that the reduced FAO and impaired TG secretion may contribute to hepatic lipid accumulation in *Arid1a*^{LKO} mice.

3.4. Arid1a deficiency augments FFA-induced lipid accumulation and insulin resistance in vitro

To directly explore the role of *Arid1a* in FAO process, we investigated whether *Arid1a* can regulate free fatty acids (FFA)-induced lipid accumulation and insulin signaling in the hepatocytes isolated from *Arid1a*$^{F/F}$ mice, where *Arid1a* was deleted by adenovirus containing *Cre* (Ad-Cre) infection (Fig. 4a). Interestingly, *Arid1a* deficiency significantly augmented the oleic acid (OA, the unsaturated fatty acid) and palmitic acid (PA, the saturated fatty acid) -induced lipid accumulation in these hepatocytes (Fig. 4b), indicating that *Arid1a* was required for FAO process to break down these saturated and unsaturated fatty acid molecules. Later on, we assessed the alterations of insulin response in the primary hepatocytes with *Arid1a* loss. The results showed that, regardless of the presence or absence of OA, *Arid1a* deficiency led to decreased phosphorylation levels of Akt and Gsk-3β in hepatocytes upon insulin stimulation (Fig. 4c). Similar results were observed in hepatocytes isolated from tamoxifen-induced *Arid1a* knockout mice, as well as in hepatocellular carcinoma (HCC) cell lines MHCC-97H and SK-Hep1-6 with *Arid1a* knockout by CRISPR-Cas9 system upon insulin treatment (Supplementary Fig. 4).

Next, we performed the rescue assay on the *Arid1a*$^{-/-}$ primary mouse hepatocytes via ectopic ARID1A expression. Remarkably, the rescued ARID1A expression resulted in the restoration of lipid clearance in *Arid1a*-deficient hepatocytes under both OA and PA challenge, which was evidenced by quantitative analysis of Oil Red O staining (Fig. 4d and 6f). Furthermore, the phosphorylation levels of Akt and Gsk-3β were also significantly recovered by ectopic ARID1A expression, and similar results were acquired in the MHCC-97H cells with *Arid1a* deletion (Fig. 4e and f). Altogether, these data indicate that Arid1a may disrupt the fatty acid β-oxidation as a critical process for lipid metabolism regulation.

3.5. Arid1a loss down-regulates essential genes in FAO and Ppar signaling pathways

Then we performed RNA sequencing on the mouse hepatocytes infected with Ad-Cre or Ad-GFP to figure out the *Arid1a*-regulated downstream genes. Significantly, pathway analysis using the GO and KEGG databases revealed that the down-regulated genes induced by *Arid1a* deficiency were enriched in lipid and fatty acid metabolic processes, PPAR and insulin signaling pathways, respectively (Fig. 5a and b).

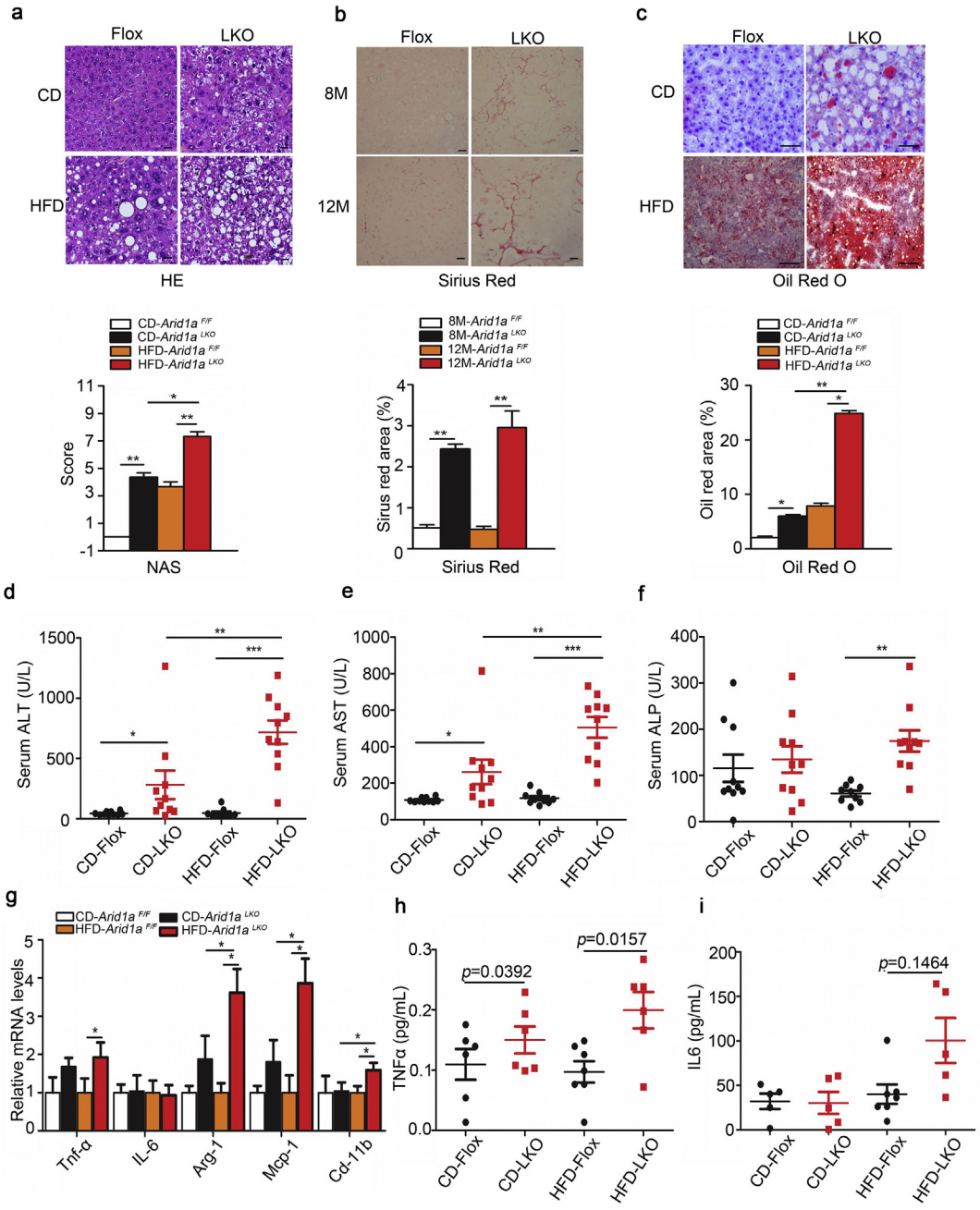

Fig. 2. HFD aggravates *Arid1a* deficiency-induced hepatic steatosis, fibrosis and inflammation. (a) Upper, H&*E*-stained histological images of liver sections from CD and HFD-fed *Arid1a*^{LKO} and *Arid1a*$^{F/F}$ mice; Down, NAS scores for *Arid1a*^{LKO} and *Arid1a*$^{F/F}$ mice at 4 months of age. Scale bar, 50 μm. (b) Upper, representative images of Sirius red-stained liver sections from HFD-fed *Arid1a*^{LKO} and *Arid1a*$^{F/F}$ mice; Down, fibrosis area was quantified. Scale bar, 50 μm. (c) Lipid droplets visualized by Oil Red O staining in livers; Down, lipid droplet area was quantified. Scale bar, 50 μm. (d-f) Serum levels of ALT (d), AST (e) and AFP (f) of male mice with the indicated diet and genotypes (n = 9–10). (g) qPCR analysis of inflammatory genes in livers of mice fed a CD or HFD (*n* = 5–8). (h-i) Serum levels of TNFα (h) and IL-6 (i) in mice fed a CD or HFD for 12 weeks (n = 5–7). Statistical analysis was performed. Values are mean ± SD. (* $P < .05$; ** $P < .01$; *** $P < .001$).

Additionally, we performed the gene set enrichment analysis and found that fatty acid metabolism was among the Top5 ranked 'Hallmark' gene sets (Fig. 5c and Supplementary Fig. 5). Many genes related to fatty acid metabolism and PPAR signaling pathways were downregulated in the *Arid1a* deficient group (Fig. 5d), some of which were consistent with qRT-PCR results in the mouse liver (Fig. 3h), suggesting that *Arid1a* loss induces the dysregulated lipid metabolism and PPAR function.

We further validated some RNA-seq revealed differentially expressed genes in hepatocytes by qRT-PCR, showing that *Arid1a* deficiency caused a significant reduction of FAO genes, such as *Pparα*, *Acox1*, *Cpt1α*, and *Hmgcs2*, in the primary mouse hepatocytes (Fig. 6a) and immortalized hepatocytes with SV40 expression (Supplementary Fig. 6). In contrast, the mRNA levels of lipogenic genes, including *Acc1, Chrebp, Srebp1c* and *Fas*, were not obviously changed in hepatocytes with *Arid1a* deletion. Moreover, the mRNA expression levels of key gluconeogenic enzymes were determined. As shown in Fig. 6A, glucose 6-phosphatase (*G6pase*), but not phosphoenolpyruvate carboxykinase (*Pepck*) mRNAs was increased 2.5-fold in the hepatocytes with *Arid1a* deficiency (Fig. 6a). qRT-PCR and western blotting assay also revealed that insulin receptor substrate 1 (*Irs1*) was significantly down-regulated in mouse hepatocytes as well as in MHCC-97H cells with *Arid1a* knockout (Supplementary information, Fig. 7). Consistently, ectopic ARID1A expression recovered the expression of *Acox1*, *Cpt1a*, *Hmgcs2*, *Peci* and *Pgc1α* in the mouse hepatocytes with *Arid1a* deletion (Fig. 6b).

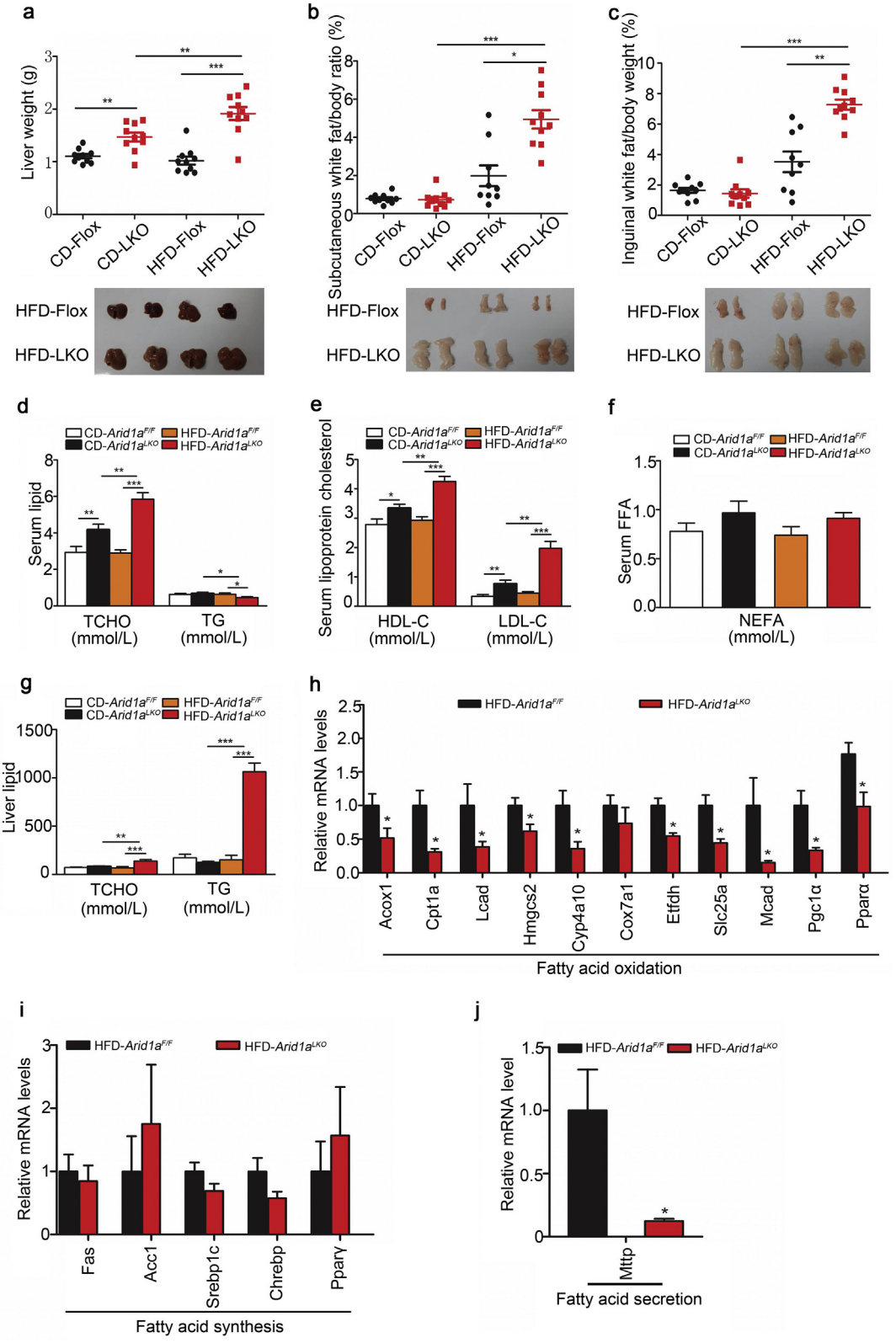

Fig. 3. *Arid1a* deprivation causes severe lipid accumulation by impairing FAO. (a) Upper, determination of liver weights of $Arid1a^{LKO}$ and $Arid1a^{F/F}$ mice at 4-month old; Down, representative images of livers of $Arid1a^{LKO}$ and $Arid1a^{F/F}$ mice fed a HFD (n = 10). (b-c) Upper, determination of subcutaneous WAT (b) and inguinal WAT (c) weights of $Arid1a^{LKO}$ and $Arid1a^{F/F}$ mice; Down, representative images of subcutaneous WAT and inguinal WAT of mice fed a HFD (n = 9–10). (d-f) TG, TCHO (d), lipoprotein-cholesterol (e) and NEFA (f) concentrations in the serum of $Arid1a^{LKO}$ and $Arid1a^{F/F}$ mice (n = 7–10). (g) Analysis of TG and TCHO contained in the livers (n = 7–10). (h-j) Real-time PCR analysis of genes involved in fatty acid oxidation (h), synthesis (i) and secretion (j) processes (n = 7). Statistical analysis was performed. Values are mean ± SD. (* $P < .05$; ** $P < .01$; *** $P < .001$).

Among the mentioned effector genes of Arid1a, we paid particularly attention to *Pparα*, the major regulator of fatty acid oxidation [25], which was largely reduced on both mRNA and protein levels in the liver and hepatocytes without *Arid1a* (Fig. 6a and c). Remarkably, western blotting assay confirmed that Pparα was recovered by ectopic ARID1A expression in the $Arid1a^{-/-}$ hepatocytes (Fig. 6d), suggesting

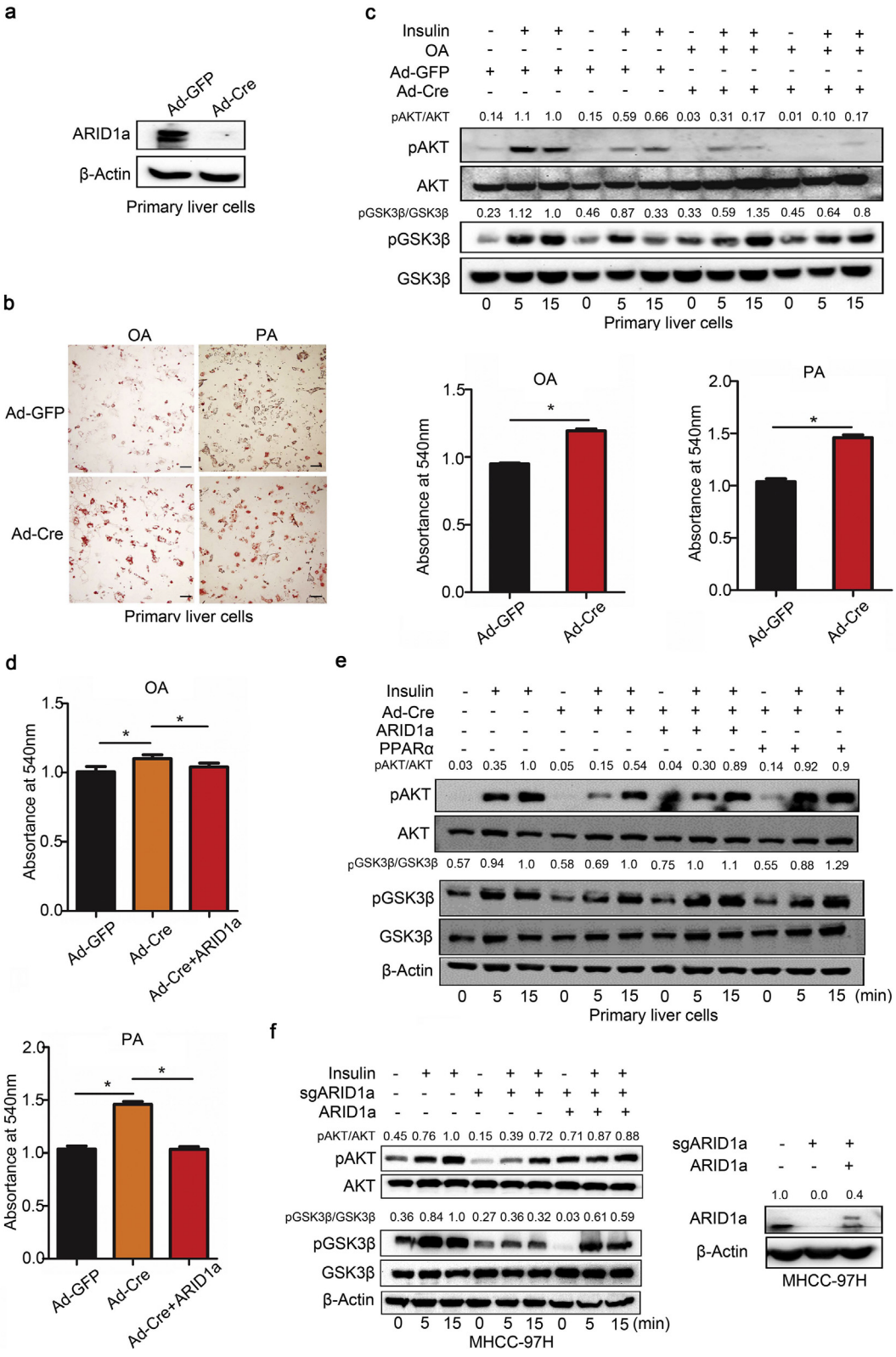

Fig. 4. *Arid1a* deficiency aggravates FFA-induced lipid accumulation and attenuates insulin sensitivity in hepatocytes. (a) Western blotting confirmed that *Arid1a* was deleted in hepatocytes infected with Ad-Cre. (b) Left, representative images of Oil Red O staining in Ad-GFP or Ad-Cre transfected hepatocytes with oleic acid (OA) or palmitic acid (PA) stimulation; Right, lipid content analysis. (c) Phosphorylation levels of Akt at serine 473 and Gsk-3β at serine 9 were assessed in hepatocytes with or without OA stimulation. (d) Ectopic ARID1A expression reverses lipid accumulation in *Arid1a*$^{-/-}$ hepatocytes. (e-f) ARID1A restoration reverses insulin resistance in hepatocytes (e) and MHCC-97H cell lines (f) with *ARID1A* deletion. Statistical analysis was performed. Values are mean ± SD. (* $P < .05$).

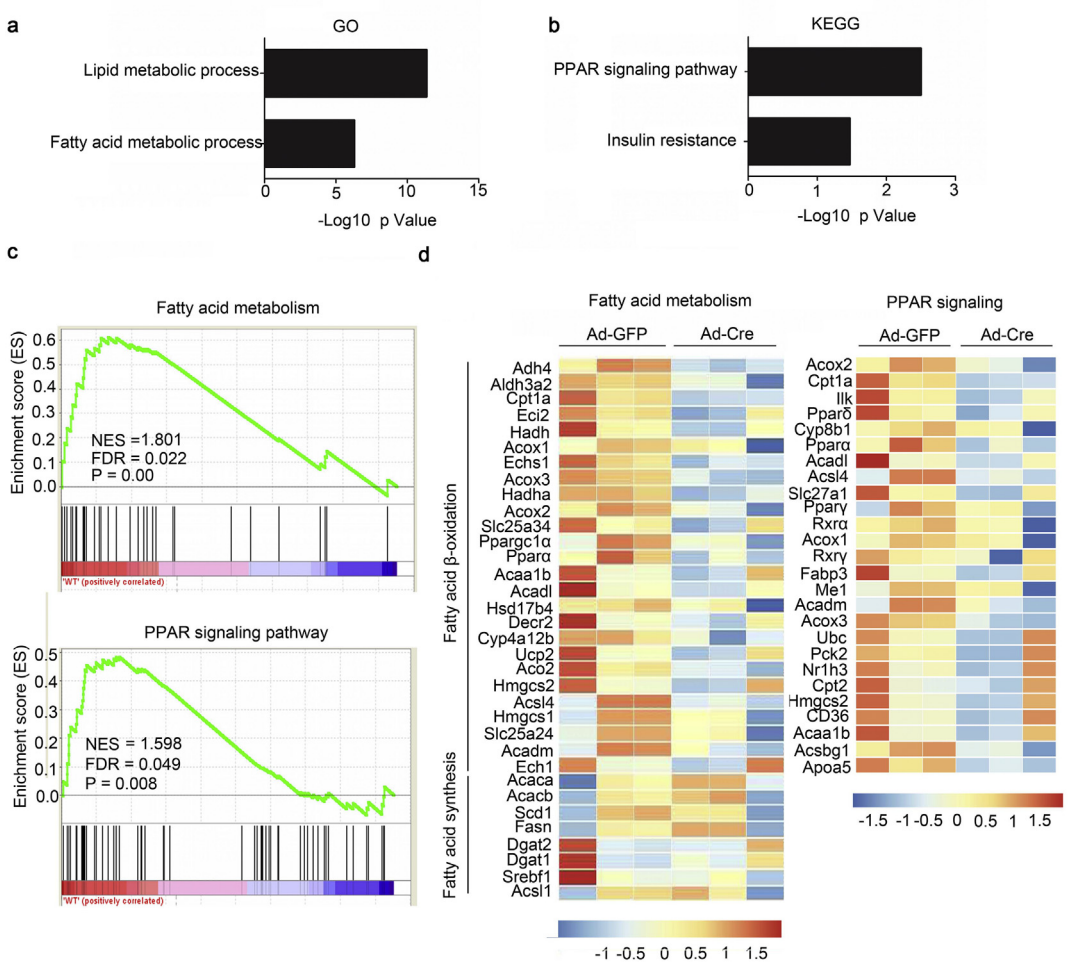

Fig. 5. *Arid1a* deprivation causes defects in lipid metabolic process and PPAR signaling. (a-b) GO (a) and KEGG (b) pathway analysis of the down-regulated genes based on RNA-seq data of *Arid1a*-deficient hepatocytes. (c) GSEA showed downregulation of the genes related to fatty acid metabolism and PPAR signaling pathways in *Arid1a*-deficient hepatocytes. (d) Heat map of mRNA levels of the genes involved in fatty acid metabolism and PPAR signaling. Red and blue depict higher and lower gene expression, respectively. Colour intensity indicates magnitude of expression differences (n = 3).

that the down-regulated *Pparα* might be critical for *Arid1a* deletion-induced lipid accumulation and insulin resistance. Later on, we investigated whether induction of PPARα can improve FAO in *Arid1a*$^{-/-}$ hepatocytes. Interestingly, the results showed that the enforced expression of PPARα, but not PPARγ partially recovered the defective expression of its downstream target genes *Acox1*, *Cpt1a*, and *Hmgcs2* in *Arid1a*$^{-/-}$ hepatocytes (Fig. 6e and Supplementary information, Fig. 8). Consequently, ectopic PPARα expression alleviated the lipid accumulation induced by OA and PA (Fig. 6f), and insulin sensitivity, indicated by pAKT and pGSK3β in mouse *Arid1a*$^{-/-}$ hepatocytes (Fig. 4e). The results testified that *Arid1a* deficiency-induced transcription repression of Pparα and related fatty acid oxidation genes could be responsible for hepatic lipid accumulation and steatosis. Furthermore, given the downregulated expression of MTTP in *Arid1a*^{LKO} mice, we speculated that MTTP might also have a role in *Arid1a* deletion-induced lipid accumulation. Therefore, we overexpressed MTTP in the *Arid1a*$^{-/-}$ hepatocytes and observed recovered lipid clearance in these cells with OA and PA treatment, implying impaired VLDL secretion also participated in *Arid1a* deficiency-induced lipid accumulation (Fig. 6g).

3.6. Arid1a deficiency decreases H3K4me3 and chromatin accessibility on promoters of metabolic genes

It is noteworthy that Arid1a may facilitate accesses of transcription factors and regulatory proteins to the genomic DNA, and thus regulates the transcription of downstream genes. Therefore, we proposed that Arid1a might impact on the local epigenetic landscape to regulate transcription activity of key metabolic genes. Here, we firstly analyzed the published ChIP-seq dataset for Arid1a from primary hepatocytes (GSE65167) [26]. Bioinformatic analysis based on GO and KEGG databases indicated that the Arid1a target genes are highly associated with lipid, fatty acid metabolic processes and PPAR signaling (Fig. 7a and b). Then we integrated the *Arid1a*-regulated genes, indicated by RNA-seq data, in mouse hepatocytes, with the genes containing Arid1a-binding peaks on promoter (Supplementary information, Fig. 9), showing that two key FAO related genes *Acox1* and *Cpt1a* have the Arid1a-binding peaks (Fig. 7c). Notably, Cpt1a is a rate-limiting enzyme involved in mitochondrial β-oxidation, catalyzing the esterification of long-chain acyl-CoAs to L-carnitine for their transportation into the mitochondria [27]. While Acox1 is the first and a rate-limiting enzyme in the peroxisomal β-oxidation which catalyzing the desaturation of very-long-chain acyl-CoAs to 2-trans-enoyl-CoAs [28]. To verify the binding of Arid1a to their promoters, we performed ChIP-PCR with anti-Arid1a antibody in primary hepatocytes with or without *Arid1a*. Our results showed that Arid1a was present in the promoters of *Acox1* and *Cpt1a* in hepatocytes with *Arid1a*, but this occupancy was decreased in *Arid1a*-deficient cells (Fig. 7d). We further explored whether Arid1a can epigenetically regulate fatty acid oxidation-related genes. Before the experiment, we analyzed the published ChIP-seq dataset for trimethylation of H3 lysine 4 from liver (H3K4me3, GSE77625), an epigenetic marker associated with transcriptional activation, to see which genes contain H3K4me3-binding peaks on their promoters. It turned

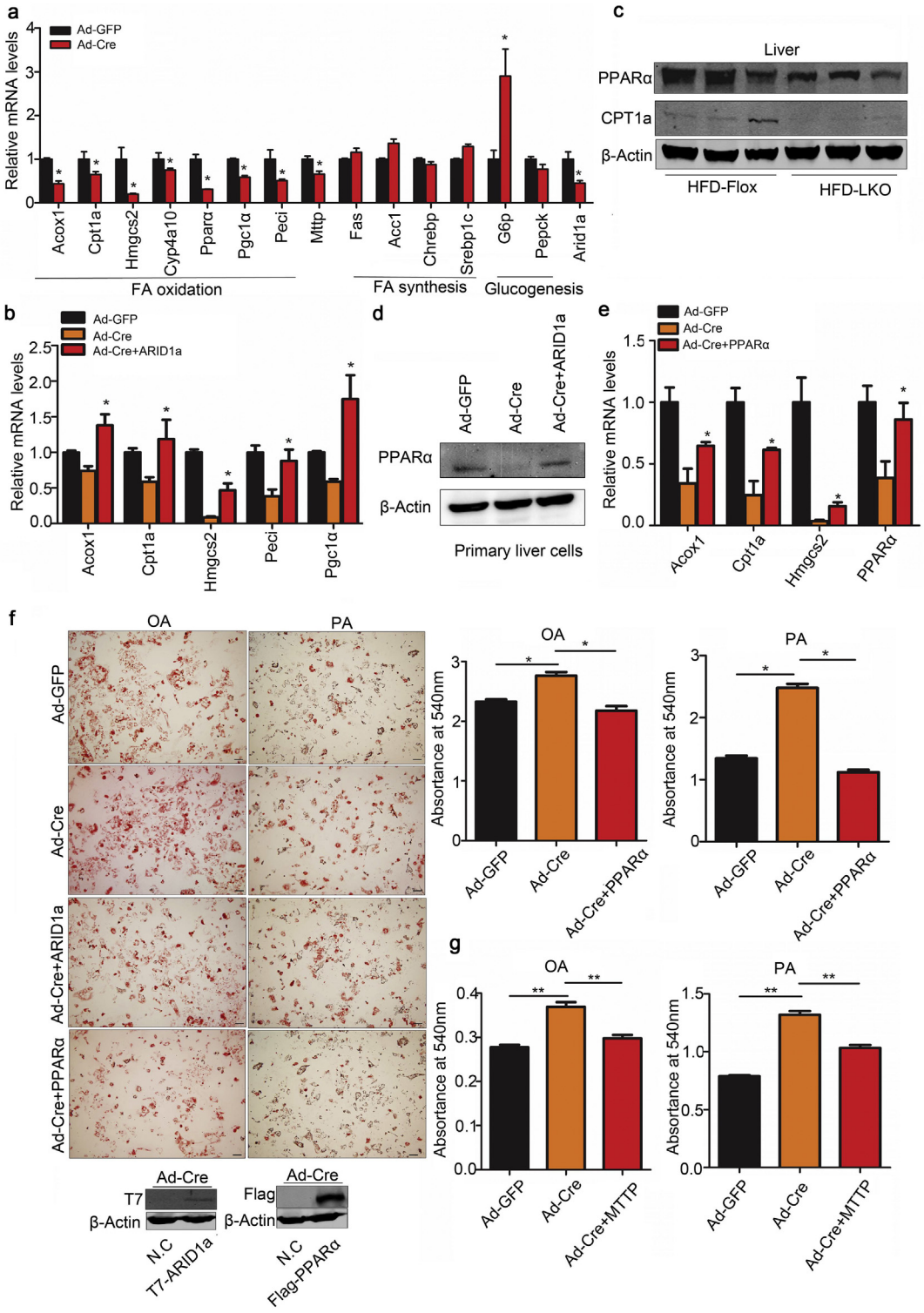

Fig. 6. Ectopic PPARα expression protects against FAO impairment and lipid accumulation in hepatocytes with *Arid1a* deletion. (a) Real-time analysis of the gene expression involved in lipid or glucose metabolism in hepatocytes transfected with Ad-GFP or Ad-Cre. (b) Ectopic ARID1A expression stimulates mRNA levels of fatty acid oxidation-related genes in *Arid1a*$^{-/-}$ hepatocytes. (c) Western blotting analysis of Pparα and Cpt1a expression in mouse livers (n = 3). (d) PPARα expression was restored by ARID1A overexpression in *Arid1a*$^{-/-}$ hepatocytes. (e) *Arid1a* deletion-induced *Cpt1a* and *Acox1* downregulation was partially abrogated by PPARα overexpression in hepatocytes. (f) Upper left, lipid droplets visualized by Oil Red O staining in hepatocytes; Right, quantitation of lipid content in hepatocytes; Down left, Overexpression of PPARα and ARID1a in hepatocytes transfected with Ad-Cre. (g) Ectopic MTTP expression reversed lipid accumulation in *Arid1a*$^{-/-}$ hepatocytes with oleic acid (OA) or palmitic acid (PA) stimulation. Statistical analysis was performed. Values are mean ± SD. (* $P < .05$).

out that Acox1 and Cpt1a, two key rate-limiting enzymes of fatty acid oxidation, have the H3K4me3 binding sites on their promoters. We further verified this hypothesis via ChIP-PCR with anti-H3K4me3 antibody, on *Acox1* and *Cpt1a* promoters. As expected, H3K4me3 on these regions was significantly reduced with *Arid1a* loss (Fig. 7e). Furthermore, *Arid1a* deficiency diminished the recruitment of SWI/SNF core subunit Brg1 to the promoter of *Cpt1a*, indicated by ChIP-PCR with anti-Brg1 antibody (Fig. 7f). Next, we conducted ATAC-seq to assess the alterations in

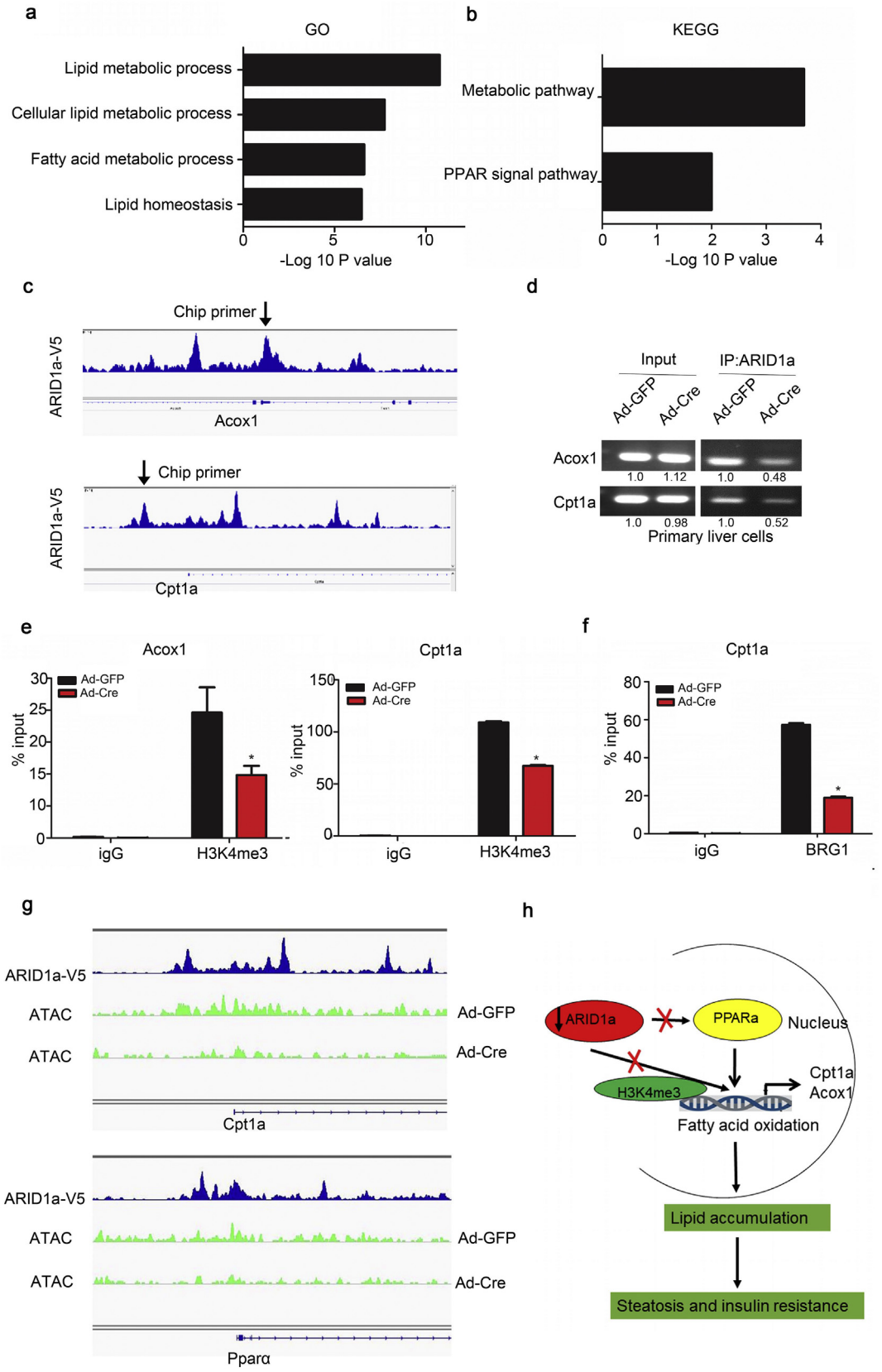

Fig. 7. *Arid1a* deletion leads to the decreased H3K4me3 and chromatin accessibility to the metabolic genes promoter. (a–b) GO (a) and KEGG (b) pathway analysis of *Arid1a*-targeted genes identified by ChIP-Seq. (c-d) ChIP-seq (c) and ChIP-PCR (d) analysis of Arid1a-binding affinity in *Cpt1a* and *Acox1* promoter (*$P < .05$). (e) ChIP-qPCR analysis of H3K4me3-binding affinity in *Cpt1a* and *Acox1* promoter. Values are mean ± SD (*$P < .05$). (f) ChIP-qPCR analysis of BRG1-binding affinity in *Cpt1a* promoter. Values are mean ± SD. (*$P < .05$). (g) ATAC-seq profiles show that chromatin accessibility at *Cpt1a* and *Pparα* promoters is affected by *Arid1a* depletion. (h) The proposed model for the role of Arid1a loss in hepatic steatosis and insulin resistance. Arid1a normally facilitates fatty acid oxidation by directly altering the epigenetic modification of H3K4me3 on the lipid metabolism-related genes, such as *Cpt1a, Acox1*, as well as by indirectly activating the master transcriptional factor Pparα, resulting in transcriptional activation of these FAO-associated genes, thereby maintaining lipid and glucose homeostasis. Arid1a loss disrupts the epigenetic landscape and Pparα-mediated transcription of FAO-related genes, resulting in hepatic steatosis and insulin resistance.

chromatin accessibility on the promoters of *Acox1*, *Cpt1a* and *Pparα*. Notably, statistical analysis on the ATAC-seq data indicated that the chromatin accessibilities on promoters of *Pparα, as well as Cpt1α* were significantly reduced when *Arid1a* was deleted in the hepatocytes (Fig. 7g). Altogether, these results indicate that Arid1a facilitates fatty acid oxidation by directly altering the epigenetic landscape of metabolism gene loci, including chromatin accessibility and local histone modification, as well as by indirectly activating downstream genes through Pparα transcription factor. *Arid1a* deficiency may result in transcriptional reduction of these FAO associated genes, thereby attenuating the corresponding metabolic functions that ends to hepatic steatosis, and insulin resistance (Fig. 7h).

4. Discussion

The liver plays a unique role in the regulation of glucose and lipid homeostasis. A central issue in understanding metabolic regulation is the definition of regulators involved in this process. Here, we identified an epigenetic modulator, Arid1a, that directly regulates essential metabolic genes in liver tissues to maintain glucose and lipid homeostasis. Hepatic *Arid1a*-deficient mice developed insulin resistance, hyperlipidemia, and morphologic alterations in the liver. In vitro, *Arid1a* deletion in hepatocytes aggravated FFA-induced lipid accumulation and attenuated insulin sensitivity. At the mechanistic level, hepatic Arid1a is critical for maintaining lipid and glucose metabolic homeostasis through Pparα-mediated fatty acid oxidation in the liver. From a clinical perspective, these data indicate that targeting ARID1A might be a promising therapeutic strategy for treating metabolic related disorders.

Several lines of evidences supported a pivotal role of Arid1a in metabolic regulation. First, the transcriptional profiling and pathway analysis indicated that the genes involved in lipid metabolism, especially fatty acid metabolism were among the top down-regulated by *Arid1a* deletion. Second, mRNA levels of the genes responsible for fatty acid oxidation were significantly reduced in *Arid1a*$^{-/-}$ livers and hepatocytes. Third, Arid1a downregulates *Pparα*, the major transcriptional factor for FAO [29]. Consistently, Pparα overexpression in *Arid1a*$^{-/-}$ hepatocytes was sufficient to eliminate the lipid accumulation and insulin resistance phenotypes in vitro. Moreover, Arid1a regulates transcription activity of key metabolic genes on the local epigenetic landscape. Specifically, *Arid1a* deficiency leads to reduced levels of H3K4me3 and compacted chromatin structure on promoters of key metabolic genes.

Previous studies demonstrated that SWI/SNF family member BAF60c, recruiting other subunits, including ARID1A, interacted with USF transcription factor to lipogenic gene promoters to increase lipogenesis in response to feeding/insulin treatment [8]. Recently, Moore et al. just demonstrated that liver-specific *Arid1a* deficiency lead to the fatty liver disease by directly regulating target genes in both the lipogenic and FAO pathways [18]. Whereas we showed that *Arid1a* loss increased susceptibility to develop liver steatosis and insulin resistance by downregulating expression of these genes involved in FAO rather than de novo lipogenesis pathway. Especially, the expression of Cpt1a and Acox1, two key rate-limiting enzymes in fatty acid oxidation, were largely reduced with *Arid1a* loss. Mechanically, Moore et al. employed a Srebp inhibitor to prove the importance of lipogenesis in the *Arid1a*/*Pten* double knockout model. Instead, we isolated primary liver cells to directly explore the role of Arid1a in FAO process, illustrating that Arid1a regulated lipid homeostasis by binding promoter sequences and altering accessibility to transcriptional machinery. It has been reported that the disorders of hepatic fatty acid oxidation lead to massive steatosis and hypertriglyceridemia in animals. Some emerging evidences have shown that hepatic FAO is also impaired in human liver disease [30–32]. Moreover, compared with control mice, *Pparα*-deficient mice developed massive steatosis, lobular inflammation, and insulin resistance due to an impairment of mitochondrial FAO, and increment of oxidative stress and inflammation [33–35]. We identified that *Pparα* expression was downregulated in hepatocytes and mice with *Arid1a* deletion, and overexpression of Pparα restored lipid accumulation and insulin resistance caused by *Arid1a* deficiency. Unfortunately, although by analyzing ChIP-seq data performed by others [26], Pparα contains Arid1a-binding sites on its promoter, no such direct binding of Arid1a on *Pparα* promoter was identified in our experiment. In addition, we also did not detect any physical association between ARID1A and PPARα in 293 T cells (data was not shown).

In summary, this study demonstrates that hepatocyte-specific inactivation of *Arid1a* reduced fatty acid oxidation, and aggravated diet-induced steatosis and insulin resistance in mice. Arid1a downregulates expression of the genes involved in fatty acid oxidation through Pparα and epigenetic regulation. These findings reveal a new mechanism underlying the role of Arid1a in glucose and lipid metabolism, and suggest a promising target for the treatment of hepatic steatosis, fibrosis and insulin resistance by modulating Arid1a.

Declarations of interests

All authors have nothing to disclose.

Author contributions

Ze-Guang Han conceived and supervised the study.

Yu-lan Qu designed and performed experiments, analyzed data, wrote manuscript. Chuan-Huai Deng and Lan Wang did literature search and performed the experiments with primary hepatocytes.

Qing Luo, Yi shi and Xue-Ying Shang performed bioinformatics analysis on data collected through RNA seq, ChIP-Seq and ATAC-Seq.

Jiao-Xiang Wu performed the experiments of lipid accumulation on hepatocytes upon OA and PA treatment.

Funding and acknowledgment

This work was supported by grants from National Natural Science Foundation of China (81672772 and 81472621), China National Science and Technology Major Project for Prevention and Treatment of Infectious Diseases (No.2017ZX 10203207) and National Program on Key Research Project of China (grant no. 2016YFC0902701). *Arid1a*$^{F/F}$ mice were provided by Zhong Wang professor (Cardiovascular Research Center of Harvard Medical School). Funders had no role in study design, data interpretation and writing of the manuscript.

Appendix A. Supplementary data

Supplementary data to this article can be found online at https://doi.org/10.1016/j.ebiom.2019.03.021.

References

[1] Fang JZ, Li C, Liu XY, Hu TT, Fan ZS, Han ZG. Hepatocyte-specific Arid1a deficiency initiates mouse steatohepatitis and hepatocellular carcinoma. PLoS One 2015;10(11):e0143042. https://doi.org/10.1371/journal.pone.0143042.
[2] Samuel VT, Shulman GI. Nonalcoholic fatty liver disease as a nexus of metabolic and hepatic diseases. Cell Metab 2018;27(1):22–41. https://doi.org/10.1016/j.cmet.2017.08.002.
[3] Fritz IB, Yue KT. Long-chain carnitine acyltransferase and the role of acylcarnitine derivatives in the catalytic increase of fatty acid oxidation induced by carnitine. J Lipid Res 1963;4:279–88.
[4] Demir M, Lang S, Steffen HM. Nonalcoholic fatty liver disease - current status and future directions. J Dig Dis 2015;16(10):541–57. https://doi.org/10.1111/1751-2980.12291.
[5] Muchardt C, Yaniv M. ATP-dependent chromatin remodelling: SWI/SNF and co. are on the job. J Mol Biol 1999;293(2):187–98. https://doi.org/10.1006/jmbi.1999.2999.
[6] Wilson BG, Roberts CW. SWI/SNF nucleosome remodellers and cancer. Nat Rev Cancer 2011;11(7):481–92. https://doi.org/10.1038/nrc3068.
[7] Gresh L, Bourachot B, Reimann A, Guigas B, Fiette L, Garbay S, et al. The SWI/SNF chromatin-remodeling complex subunit SNF5 is essential for hepatocyte differentiation. EMBO J 2005;24(18):3313–24. https://doi.org/10.1038/sj.emboj.7600802.
[8] Wang Y, Wong RH, Tang T, Hudak CS, Yang D, Duncan RE, et al. Phosphorylation and recruitment of BAF60c in chromatin remodeling for lipogenesis in response to insulin. Mol Cell 2013;49(2):283–97. https://doi.org/10.1016/j.molcel.2012.10.028.

[9] Meng ZX, Li S, Wang L, Ko HJ, Lee Y, Jung DY, et al. Baf60c drives glycolytic metabolism in the muscle and improves systemic glucose homeostasis through Deptor-mediated Akt activation. Nat Med 2013;19(5):640–5. https://doi.org/10.1038/nm.3144.
[10] Meng ZX, Wang L, Chang L, Sun J, Bao J, Li Y, et al. A diet-sensitive BAF60a-mediated pathway links hepatic bile acid metabolism to cholesterol absorption and atherosclerosis. Cell Rep 2015;13(8):1658–69. https://doi.org/10.1016/j.celrep.2015.10.033.
[11] Li S, Liu C, Li N, Hao T, Han T, Hill DE, et al. Genome-wide coactivation analysis of PGC-1alpha identifies BAF60a as a regulator of hepatic lipid metabolism. Cell Metab 2008;8(2):105–17. https://doi.org/10.1016/j.cmet.2008.06.013.
[12] Dallas PB, Cheney IW, Liao DW, Bowrin V, Byam W, Pacchione S, et al. p300/CREB binding protein-related protein p270 is a component of mammalian SWI/SNF complexes. Mol Cell Biol 1998;18(6):3596–603. https://doi.org/10.1128/MCB.18.6.3596.
[13] Dallas PB, Pacchione S, Wilsker D, Bowrin V, Kobayashi R, Moran E. The human SWI-SNF complex protein p270 is an ARID family member with non-sequence-specific DNA binding activity. Mol Cell Biol 2000;20(9):3137–46. https://doi.org/10.1128/MCB.20.9.3137-3146.2000.
[14] Martens JA, Winston F. Recent advances in understanding chromatin remodeling by Swi/Snf complexes. Curr Opin Genet Dev 2003;13(2):136–42. https://doi.org/10.1016/S0959-437X(03)00022-4.
[15] Nagl Jr NG, Zweitzig DR, Thimmapaya B, Beck Jr GR, Moran E. The c-myc gene is a direct target of mammalian SWI/SNF-related complexes during differentiation-associated cell cycle arrest. Cancer Res 2006;66(3):1289–93. https://doi.org/10.1158/0008-5472.CAN-05-3427.
[16] Trotter KW, Archer TK. Reconstitution of glucocorticoid receptor-dependent transcription in vivo. Mol Cell Biol 2004;24(8):3347–58. https://doi.org/10.1128/MCB.24.8.3347-3358.2004.
[17] Trotter KW, Fan HY, Ivey ML, Kingston RE, Archer TK. The HSA domain of BRG1 mediates critical interactions required for glucocorticoid receptor-dependent transcriptional activation in vivo. Mol Cell Biol 2008;28(4):1413–26. https://doi.org/10.1128/MCB.01301-07.
[18] Moore A, Wu L, Chuang JC, Sun X, Luo X, Gopal P, et al. Arid1a loss drives non-alcoholic steatohepatitis in mice via epigenetic dysregulation of hepatic lipogenesis and fatty acid oxidation. Hepatology 2018. https://doi.org/10.1002/hep.30487.
[19] Kegel V, Deharde D, Pfeiffer E, Zeilinger K, Seehofer D, Damm G. Protocol for isolation of primary human hepatocytes and corresponding major populations of non-parenchymal liver cells. J Vis Exp 2016(109):e53069. https://doi.org/10.3791/53069.
[20] Trapnell C, Pachter L, Salzberg SL. TopHat: discovering splice junctions with RNA-Seq. Bioinformatics 2009;25(9):1105–11. https://doi.org/10.1093/bioinformatics/btp120.
[21] Roberts A, Trapnell C, Donaghey J, Rinn JL, Pachter L. Improving RNA-Seq expression estimates by correcting for fragment bias. Genome Biol 2011;12(3):R22. https://doi.org/10.1186/gb-2011-12-3-r22.
[22] Subramanian A, Tamayo P, Mootha VK, Mukherjee S, Ebert BL, Gillette MA, et al. Gene set enrichment analysis: a knowledge-based approach for interpreting genome-wide expression profiles. Proc Natl Acad Sci U S A 2005;102(43):15545–50.
[23] Buenrostro JD, Wu B, Chang HY, Greenleaf WJ. ATAC-seq: a method for assaying chromatin accessibility genome-wide. Curr Protoc Mol Biol 2015;109 (21 9 1-9).
[24] Fabbrini E, Sullivan S, Klein S. Obesity and nonalcoholic fatty liver disease: biochemical, metabolic, and clinical implications. Hepatology 2010;51(2):679–89. https://doi.org/10.1002/hep.23280.
[25] Leone TC, Weinheimer CJ, Kelly DP. A critical role for the peroxisome proliferator-activated receptor alpha (PPARalpha) in the cellular fasting response: the PPARalpha-null mouse as a model of fatty acid oxidation disorders. Proc Natl Acad Sci U S A 1999;96(13):7473–8.
[26] Sun X, Chuang JC, Kanchwala M, Wu L, Celen C, Li L, et al. Suppression of the SWI/SNF component Arid1a promotes mammalian regeneration. Cell Stem Cell 2016;18(4):456–66. https://doi.org/10.1016/j.stem.2016.03.001.
[27] Bergman AJ, Donckerwolcke RA, Duran M, Smeitink JA, Mousson B, Vianey-Saban C, et al. Rate-dependent distal renal tubular acidosis and carnitine palmitoyltransferase I deficiency. Pediatr Res 1994;36(5):582–8. https://doi.org/10.1203/00006450-199411000-00007.
[28] Zeng J, Li D. Expression and purification of his-tagged rat peroxisomal acyl-CoA oxidase I wild-type and E421 mutant proteins. Protein Expr Purif 2004;38(1):153–60. https://doi.org/10.1016/j.pep.2004.08.013.
[29] McGarry JD, Foster DW. Regulation of hepatic fatty acid oxidation and ketone body production. Annu Rev Biochem 1980;49:395–420. https://doi.org/10.1146/annurev.bi.49.070180.002143.
[30] Samuel VT, Shulman GI. Mechanisms for insulin resistance: common threads and missing links. Cell 2012;148(5):852–71. https://doi.org/10.1016/j.cell.2012.02.017.
[31] Schmid AI, Szendroedi J, Chmelik M, Krssak M, Moser E, Roden M. Liver ATP synthesis is lower and relates to insulin sensitivity in patients with type 2 diabetes. Diabetes Care 2011;34(2):448–53. https://doi.org/10.2337/dc10-1076.
[32] Cortez-Pinto H, Chatham J, Chacko VP, Arnold C, Rashid A, Diehl AM. Alterations in liver ATP homeostasis in human nonalcoholic steatohepatitis: a pilot study. Jama 1999;282(17):1659–64. https://doi.org/10.1001/jama.282.17.1659.
[33] Ip E, Farrell GC, Robertson G, Hall P, Kirsch R, Leclercq I. Central role of PPARalpha-dependent hepatic lipid turnover in dietary steatohepatitis in mice. Hepatology 2003;38(1):123–32. https://doi.org/10.1053/jhep.2003.50307.
[34] Abdelmegeed MA, Yoo SH, Henderson LE, Gonzalez FJ, Woodcroft KJ, Song BJ. PPARalpha expression protects male mice from high fat-induced nonalcoholic fatty liver. J Nutr 2011;141(4):603–10. https://doi.org/10.3945/jn.110.135210.
[35] Su Q, Baker C, Christian P, Naples M, Tong X, Zhang K, et al. Hepatic mitochondrial and ER stress induced by defective PPARalpha signaling in the pathogenesis of hepatic steatosis. Am J Physiol Endocrinol Metab 2014;306(11):E1264–73. https://doi.org/10.1152/ajpendo.00438.2013.